



1 Interhemispheric Effect of Global Geography on Earth's 2 Climate Response to Orbital Forcing

3 **Rajarshi Roychowdhury¹ and Robert DeConto¹**

4 ¹University of Massachusetts - Amherst

5 *Correspondence to:* roychowdhur@geo.umass.edu

6 **Postal Address:**

7 Department of Geosciences

8 627 North Pleasant Street

9 233 Morrill Science Center

10 University of Massachusetts

11 Amherst, MA 01003-9297

12 **Abstract**

13 The climate response of the Earth to orbital forcing shows a distinct hemispheric
14 asymmetry due to the unequal distribution of land in the Northern versus Southern
15 Hemispheres. This asymmetry is examined using a Global Climate Model (GCM) and a
16 Land Asymmetry Effect (LAE) is quantified for each hemisphere. The results show how
17 changes in obliquity and precession translate into variations in the calculated LAE. We
18 find that the global climate response to specific past orbits is likely unique and modified
19 by complex climate-ocean-cryosphere interactions that remain poorly known and difficult



20 to model. Nonetheless, these results provide a baseline for interpreting contemporaneous
21 proxy climate data spanning a broad range of latitudes, which maybe especially useful in
22 paleoclimate data-model comparisons, and individual time-continuous records exhibiting
23 orbital cyclicity.

24 **1. Introduction**

25 The arrangement of continents on the Earth's surface plays a fundamental role in the
26 Earth's climate response to forcing. This global "geography" is primarily the result of the
27 horizontal and vertical displacements associated with plate tectonics. While these
28 processes are ongoing, the global continental configuration has been close to its present
29 form since the mid-Cenozoic. Today, more continental land area is found in the Northern
30 Hemisphere (68%) as compared to the Southern Hemisphere (32%). These different
31 ratios of land vs. ocean in each hemisphere affect the balance of incoming and outgoing
32 radiation, atmospheric circulation, ocean currents, and the availability of terrain suitable
33 for growing glaciers and ice-sheets. As a result of this land-ocean asymmetry, the
34 climatic responses of the Northern and Southern Hemisphere differ for an identical
35 change in radiative forcing (Barron et al., 1984; Deconto et al., 2008; Kang et al., 2014;
36 Loutre, 2003; Short et al., 1991).

37 A number of classic studies have shown interhemispheric asymmetry in climate response
38 of Northern and Southern Hemispheres. Climate simulations made with coupled
39 atmosphere-ocean GCMs typically show a strong asymmetric response to greenhouse-gas
40 loading, with Northern Hemisphere high latitudes experiencing increased warming
41 compared to Southern Hemisphere high latitudes (Stouffer et al., 1989; Flato and Boer,



42 2001). GCMs also show that the Northern and Southern Hemispheres respond differently
43 to changes in orbital forcing (e.g. Philander et al., 1996). While the magnitude of
44 insolation changes through each orbital cycle is identical for both hemispheres, the
45 difference in climatic response can be attributed to the fact that Northern Hemisphere is
46 land-dominated while Southern Hemisphere is water dominated (Croll, 1870). This
47 results in a stronger response to orbital forcing in the Northern Hemisphere relative to the
48 Southern Hemisphere.

49 The changing continental configurations as a result of plate tectonics have been linked
50 with climate change over a wide range of timescales (e.g. Crowley and North, 1996;
51 DeConto, 2009; Fawcett and Barron, 1998; Hay, 1996). The distribution of continents
52 and oceans have an important effect on the spatial heterogeneity of the Earth's energy
53 balance, primarily via the differences in albedos and thermal properties of land versus
54 ocean (Trenberth et al., 2009). The latitudinal distribution of land has a dominant effect
55 on zonally averaged net radiation balance due to its influence on planetary albedo and
56 ability to transfer energy to the atmosphere through long-wave radiation, and fluxes of
57 sensible and latent heat. The latitudinal net radiation gradient controls the total poleward
58 heat transport requirement, which is the ultimate driver of winds, and ocean circulation
59 (Stone, 1978).

60 Oceans have a relatively slower response to seasonal changes in insolation due to the
61 higher specific heat of water as compared to land, and mixing in the upper ~10-150 m of
62 the ocean. As a result, in the ocean-dominated Southern Hemisphere, the surface waters
63 suppress extreme temperature swings in the winter and provide the atmosphere with a



64 source of moisture and diabatic heating. In the land-dominated Northern Hemisphere, the
65 lower heat capacity of the land combined with relatively high albedo results in greater
66 seasonality, particularly in the interiors of large continents of Asia and North America.

67 The continentality of the Northern Hemisphere manifests itself in different
68 hemispherically asymmetric climatic phenomenon, like the well-known Asian monsoonal
69 circulation system. The intertropical convergence zone (ITCZ) is considered to be the
70 region of low-level convergence and convective precipitation. The ITCZ moves further
71 away from the equator during the Northern summer than the Southern one due to the
72 continentality of the Northern Hemisphere (Kang et al., 2008; Philander et al., 1996).
73 The land surface available in a particular hemisphere also affects the potential for
74 widespread glaciation. The extreme cold winters associated with large continents provide
75 the means of accumulation of winter snow, while the critical factor for formation of ice-
76 sheets is annual ablation and can be estimated by the sum of Positive Degree Days (PDD)
77 in a year (e.g. Huybers, 2006).

78 Continental geography has a strong impact on polar climates, as is evident from the very
79 different climatic regimes of the Arctic and the Antarctic. Several early paleoclimate
80 modeling studies using GCMs investigated continental distribution as a forcing factor of
81 global climate (e.g. Barron et al., 1984; Hay et al., 1990). These studies demonstrated that
82 an Earth with its continents concentrated in the low latitudes is warmer and has lower
83 equator-to-pole temperature gradients than an Earth with only polar continents. Although
84 these early model simulations did not incorporate all the complexities of the climate
85 system, the results provided valuable insights from comparative studies of polar versus



86 equatorial continents in the Earth and showed that changes in continental configuration
87 has significant influence on climatic response to forcing.

88 2. Methods

89 2.1 Experimental design

90 We use the latest (2012) version of the Global ENvironmental and Ecological Simulation
91 of Interactive Systems (GENESIS) 3.0 GCM with a slab ocean component (Thompson
92 and Pollard, 1997) rather than a full-depth dynamical ocean (Alder et al., 2011). The slab-
93 ocean predicts sea surface temperatures and ocean heat transport as a function of the local
94 temperature gradient and the zonal fraction of land versus sea at each latitude. While
95 explicit changes in ocean currents and the deep ocean are not represented, the
96 computational efficiency of the slab-ocean version of the GCM allows numerous
97 simulations with idealized global geographies and greatly simplifies interpretations of the
98 sensitivity tests by precluding complications associated with ocean model dependencies.
99 In addition to the atmosphere and slab-ocean, the GCM includes model components
100 representing vegetation, soil, snow, and thermo-dynamic sea ice. The 3-D atmospheric
101 component of the GCM uses an adapted version of the NCAR CCM3 solar and thermal
102 infrared radiation code (Kiehl et al., 1998) and is coupled to the surface components by a
103 land-surface-transfer scheme (LSX). In the setup used here, the model atmosphere has a
104 spectral resolution of T31 ($\sim 3.75^\circ$) with 18 vertical layers. Land-surface components are
105 discretized on a higher resolution $2^\circ \times 2^\circ$ grid.

106 The GCM uses various geographical boundary conditions (described below) in $2^\circ \times 2^\circ$ and
107 spectral T31 grids for surface and AGCM models, respectively. For each set of



108 experiments, the model is run for 50 years. Spin-up is taken into account, and equilibrium
109 is effectively reached after about 20 years of integration. The results used to calculate
110 interhemispheric effects are averaged over the last 20 years of each simulation.
111 Greenhouse gas mixing ratios are identical in all experiments and set at preindustrial
112 levels with CO₂ set at 280 ppmv, N₂O at 288 ppbv and CH₄ at 800 ppbv. The default
113 values for CFCl₃ and CF₂Cl₂ values are set at 0 ppm. The solar constant is maintained at
114 1367 Wm⁻².

115 2.2 Asymmetric and symmetric Earth geographies

116 The GCM experiments are divided into three sets: 1) Preindustrial CONTROL 2)
117 NORTH-SYMM and 3) SOUTH-SYMM. The Preindustrial CONTROL experiments use
118 a modern global geography spatially interpolated to the model's 2°x2° surface grid
119 (Koenig et al., 2012). The geography provides the land-ice sheet-ocean mask and land-
120 surface elevations used by the GCM.

121 To simulate the climate of an Earth with meridionally symmetric geographies, we
122 created two sets of land surface boundary conditions: NORTH-SYMM and SOUTH-
123 SYMM. For the NORTH-SYMM experiments, the CONTROL experiment boundary
124 conditions are used to generate a modified GCM surface mask, by reflecting the Northern
125 Hemisphere geography (land-sea-ice mask, topography, vegetation, soil texture) across
126 the equator into the Southern Hemisphere. Similarly, in the experiment SOUTH-SYMM,
127 the land mask and geographic boundary conditions in the Southern Hemisphere are
128 mirrored in the Northern Hemisphere. The NORTH-SYMM and SOUTH-SYMM



129 boundary conditions are shown in Figure 1B and 1C, with the CONTROL (Fig. 1A) for
130 comparison.

131 3. Asymmetry in the Earth's climate

132 We begin our study by investigating the asymmetry in the Earth's climate. In our first
133 experimental setup, we run the GCM with modern day orbital configuration, i.e.
134 eccentricity is set at 0.0167, obliquity is set at 23.5° and precession such that perihelion
135 coincides with Southern Hemisphere summer. Figure 2A shows the present day summer
136 insolation intensity and Figure 2B shows present day Summer Energy for reference. The
137 Summer Energy (J) is defined as defined as:

$$138 \quad J = \sum_i \beta_i (W_i \times 86,400) \quad \dots(1)$$

139 where W_i is mean insolation measured in W/m^2 on day i , and β equals 1 when $W_i \geq \tau$ and
140 zero otherwise. $\tau = 275 W/m^2$ is taken as the assumed threshold for melting of ice at the
141 Earth's surface). Mean Summer Temperatures (ST) are calculated from the GCM as the
142 mean of the average daily temperatures for the summer months in each hemisphere (JJA
143 in Northern Hemisphere; DJF in Southern Hemisphere). Figure 2C shows the mean
144 summer temperature for a simulation with modern orbit. The zonal averages (calculated
145 for each latitude) demonstrate the inherent asymmetry in the Earth's climate between
146 Northern and Southern Hemispheres, especially evident in the higher latitudes. A better
147 indicator of the Earth's climate system, which quantifies both the intensity of summer as
148 well as the duration of the melt season, is the sum of Positive Degree Days (PDD). The
149 sum of Positive Degree-Days is calculated as:



$$150 \quad PDD = \sum_i \alpha_i T_i \quad \dots(2)$$

151 where T_i is the mean daily temperature on day i , and α is one when $T_i \geq 0^\circ\text{C}$ and zero
152 otherwise. The PDD captures the intensity as well as the duration of the melt season, and
153 has been shown to be indicative of the ice-sheet response to changes in external forcing.
154 Figure 2D shows the PDD for modern orbit, and the zonal averages are plotted in the log
155 scale. The extreme asymmetry between the Northern and Southern Hemispheres
156 observed in the summer temperatures is also evident in the calculated PDDs.

157 The observed asymmetry in the Northern and Southern Hemispheres can be attributed to
158 three primary causes: (i) variation in insolation intensity across the Northern and
159 Southern Hemispheres caused by the precession of the equinoxes (today perihelion
160 coincides with January 3, just after the December 21 solstice, leading to slightly stronger
161 summer insolation in the Southern Hemisphere); (ii) the effect of the continental
162 geography on climate; and (iii) the effect of interhemispheric continental geography on
163 climate, i.e. the effect of Northern Hemisphere continental geography on Southern
164 Hemisphere climate and vice-versa. Here, we attempt to isolate the effect of
165 interhemispheric continental geography on climate (i.e. cause (iii) above) by comparing
166 results from GCM simulations using modern versus idealized (hemispherically
167 symmetric) global geographies (Fig. 1).

168 Next, we maintain a modern orbit to test the effect of meridionally symmetric continents
169 (Fig. 2E-H). Figure 2E and 2F show the summer temperature and PDD from a simulation
170 in which the Northern Hemisphere geography is reflected in the Southern Hemisphere
171 (thus making the Earth geographically symmetric). Figure 2G and Figure 2H shows the



172 summer temperature and PDD from a hypothetical simulation with symmetric Southern
173 Hemisphere continents. Symmetric continents make the climates of Northern and
174 Southern Hemispheres almost symmetric (>95%), with some small remaining asymmetry
175 due to the current timing of perihelion with respect to the summer solstices.

176 The simulations with modern and idealized (symmetric) geographies are used to quantify
177 the different climate responses to a range of orbits. By comparing the climatic response
178 from simulations with different geographies, we isolate and estimate the effect of
179 interhemispheric continental geography and the influence of one hemisphere's geography
180 on the climate response of the opposite hemisphere.

181 **3.1 Effect of Southern Hemisphere on Northern Hemisphere climate**

182 To estimate the effect of Southern Hemisphere continental geography on the Northern
183 Hemisphere, we compare the NH climate from the CONTROL simulation (asymmetric,
184 modern orbit) and NORTH-SYMM (symmetric Northern continents in both
185 hemispheres). In these simulations, the only difference in setup is the Southern
186 Hemispheric continental distribution. Thus the differences in Northern Hemisphere
187 climate from the two simulations, if any, can be safely ascribed as the 'effect of Southern
188 Hemisphere continental geography on Northern Hemisphere climate'. We quantify this
189 interhemispheric effect of Southern Hemisphere continental geography on NH climate as:

$$190 \quad \widehat{e}_{\text{Summer Temp}} = \frac{1}{n} \sum_i^n (T_i^{\text{control}} - T_i^{\text{north}}) \quad \dots(3)$$

$$191 \quad \widehat{e}_{\text{PDD}} = \text{PDD}^{\text{control}} - \text{PDD}^{\text{north}} \quad \dots(4)$$



192 where T_i^{control} and PDD_i^{control} are the mean daily temperature on day i and PDD from the
193 control simulation, and T_i^{North} and PDD_i^{North} are the mean daily temperature on day i and
194 PDD from the simulation with the North-symmetric geography. ‘ n ’ is the number of days
195 in the summer months in each hemisphere (JJA in Northern Hemisphere; DJF in
196 Southern Hemisphere)

197 Figure 3A and 3B show the effect of Southern Hemisphere continental geography on
198 Northern Hemisphere summer temperature and PDD respectively. For the Northern
199 Hemisphere, the summer temperatures are calculated over the months of June, July, and
200 August when the insolation intensity over the Northern Hemisphere is strongest. The
201 asymmetry in the Southern Hemisphere landmasses leads to weakening of the summer
202 warming over North America and Eurasia (blue shaded regions correspond to cooling).
203 Consequently, summer temperatures over Northern Hemisphere continents are lower by
204 3-6°C relative to a symmetric Earth. There is a positive warming effect in the North-
205 Atlantic Ocean, and in general the Northern Hemisphere oceans are slightly warmer
206 relative to a symmetric Earth. The general trends in the interhemispheric effect on PDD
207 (Fig. 3B) mimic those of the summer temperatures (Fig. 3A).

208 3.2 Effect of Northern Hemisphere on Southern Hemisphere climate

209 Similarly, we estimate the effect of Northern Hemisphere continental geography on the
210 Southern Hemisphere by comparing the SH climate of the CONTROL simulation
211 (asymmetric, modern orbit) and the SOUTH-SYMM (symmetric southern continents in
212 both hemispheres). In these simulations, the differences in Southern Hemisphere climate
213 in the CONTROL and SOUTH-SYMM simulations, if any, can be ascribed as the ‘effect



214 of Northern Hemisphere continental geography on Southern Hemisphere climate'. We
215 quantify this interhemispheric effect of Northern Hemisphere continental geography on
216 SH climate as:

$$217 \quad \widehat{e_{Summer\ Temp}} = \frac{1}{n} \sum_i^n (T_i^{control} - T_i^{south}) \quad \dots(5)$$

$$218 \quad \widehat{e_{PDD}} = PDD^{control} - PDD^{south} \quad \dots(6)$$

219 where $T_i^{control}$ and $PDD_i^{control}$ are the mean daily temperature on day i and PDD from the
220 control simulation, and T_i^{south} and PDD_i^{south} are the mean daily temperature on day i and
221 PDD from the simulation with the south-symmetric geography.

222 Figure 3C and 3D show the effect of Northern Hemisphere continental geography on
223 Southern Hemisphere summer temperature and PDD, respectively. For the Southern
224 Hemisphere, the summer temperatures are calculated over the months of December,
225 January, and February when the insolation is most intense during the year. Southern
226 Hemisphere landmasses, except Antarctica, generally show a cooling response during
227 summer, due to Northern Hemisphere geography. Over Antarctica, summer temperatures
228 are higher in the control simulations than in the symmetric simulations, leading to the
229 inference that there is a warming (increase) in summer temperatures due to
230 interhemispheric effect. Also, the Southern Ocean shows a strong positive temperature
231 effect (warming) relative to a symmetric Earth, although this Southern Ocean response
232 might be different or modified if a full-depth dynamical ocean model were used.

233



234 **4. Interhemispheric effect on the Earth's climate response to orbital (astronomical)**
235 **forcing**

236 Next, we examine the effect of the opposite hemisphere on the Earth's climate response
237 to changes in obliquity (axial tilt) and precession (positions of the solstices and equinoxes
238 in relation to the eccentric orbit). The orbital parameters used in these experiments are
239 idealized and do not correspond to a specific time in Earth's history. Rather, they are
240 chosen to provide a useful framework for studying the Earth's climate response to
241 precession and obliquity. HIGH and LOW orbits approximate the highest and lowest
242 obliquity in the last three million years (Berger and Loutre, 1991). NHSP (Northern
243 Hemisphere Summer at Perihelion) and SHSP (Southern Hemisphere Summer at
244 Perihelion) orbits correspond to Northern and austral summers coinciding with
245 perihelion, respectively, and represent the two extreme configurations of precession, with
246 obliquity set at its mean value averaged over the last 3 million years. Eccentricity is set at
247 the same moderate value (mean eccentricity over the last 3 million years) for all
248 simulations. Table 1 summarizes the orbits used in the ensemble of model simulations.
249 Here, we focus only on the sum of the Positive Degree Days (PDD) calculated from our
250 simulations. PDD is a better indicator of air temperature's influence on annual ablation
251 over ice-sheets than summer temperature, since this metric captures both the intensity and
252 duration of the melt season.

253 **4.1 Interhemispheric effect on precessional (cycle) response of the Earth's climate**

254 Changes in precession primarily affect seasonal insolation intensity that is well known to
255 be out-of-phase in both hemispheres (e.g. Raymo et al., 2006). The out-of-phase summer



256 energy (J) variation is shown in Figure 4A for reference. In one precessional cycle lasting
257 ~23-kyr, the perihelion position of the Earth's orbit moves from the Northern
258 Hemisphere summer solstice (NHSP) to the Southern Hemisphere summer solstice
259 (SHSP), which are also the two extreme precessional configurations. We run the
260 simulations at these two extreme precessions, keeping all other orbital parameters
261 constant at their mean values. The difference in the calculated PDDs from the two
262 simulations (represented as $\Delta\text{PDD}_{\text{precession}}$) gives an estimate of the Earth's climate
263 response to the combined effect of the two precessional motions (wobbling of the axis of
264 rotation and the slow turning of the orbital ellipse). Figure 4B shows the precessional
265 response of the Earth in terms of PDD, and it is observed that the Northern and Southern
266 Hemisphere responses are not symmetrical. Running the same simulations with a North-
267 symmetric Earth (Fig. 4C) and a South-symmetric Earth (Fig. 4D) results in a nearly
268 symmetrical climate responses to the precessional cycle.

269 4.2 Interhemispheric effect on obliquity (cycle) response of the Earth's climate

270 In contrast to precession, obliquity alters the seasonality of insolation equally in both
271 hemispheres (Fig. 4E). A reduction in the tilt from 24.5° (HIGH) to 22° (LOW) reduces
272 annual insolation by $\sim 17 \text{ W/m}^2$ and summer insolation by $\sim 45 \text{ W/m}^2$ in the high latitudes.
273 In the tropics, summer insolation increases by up to $\sim 5 \text{ W/m}^2$. Loutre et al. (2004) among
274 others predicted that global ice volume changes at the obliquity periods could be
275 interpreted as a response to mean annual insolation and meridional insolation gradients.
276 Similar to the experimental setup described above, we ran two simulations with the
277 highest and lowest axial tilts, keeping all other orbital parameters constant at their mean
278 values. The difference in the calculated PDDs (represented as $\Delta\text{PDD}_{\text{obliquity}}$) provides an



279 estimate of the Earth's climate response to changes in tilt. Figure 4F shows $\Delta PDD_{\text{obliquity}}$
280 and the zonal averages reveal the asymmetry in the climate response to obliquity.
281 Running the same simulations with a North-symmetric Earth (Fig. 4G) and a South-
282 symmetric Earth (Fig. 4H) produces a nearly symmetrical climate response to the
283 obliquity cycle.

284 5. Quantification of the Land Asymmetry Effect (LAE)

285 5.1 Effect of Southern Hemisphere geography on Northern Hemisphere climate

286 The effect of Southern Hemisphere continental geography on Northern Hemisphere at the
287 two extreme precessional orbits is estimated using the same method described above,
288 with Interhemispheric effect of Southern Hemisphere continental geography on NH
289 climate at 'NHSP' calculated as:

$$290 \quad (\widehat{e_{PDD}})_{NHSP} = PDD_{NHSP}^{control} - PDD_{NHSP}^{north} \quad \dots(7)$$

291 and interhemispheric effect of Southern Hemisphere continental geography on NH
292 climate at 'SHSP' calculated as:

$$293 \quad (\widehat{e_{PDD}})_{SHSP} = PDD_{SHSP}^{control} - PDD_{SHSP}^{north} \quad \dots(8)$$

294 Figure 5A shows the spatial variation of $(\widehat{e_{PDD}})_{NHSP}$. The Northern Hemisphere
295 landmasses show a strong negative response to PDD when perihelion coincides with
296 Northern Hemisphere summer (NHSP). In this orbit, the Northern Hemisphere
297 experiences elevated summer insolation, but the response is weakened due to the
298 interhemispheric effect. This dampening effect is greatest in the interiors of the Northern



299 Hemisphere continents (Fig. 5A). According to Milankovitch theory, the Northern
300 Hemisphere should experience ‘interglacial’ conditions when perihelion coincides with
301 boreal summer. However, because of the interhemispheric effect, interglacial (warm
302 summer) conditions are muted relative to those on a symmetric Earth. Figure 5B shows
303 the spatial variation of $(\widehat{e_{PDD}})_{SHSP}$. When perihelion coincides with Southern
304 Hemisphere summer (SHSP), the Northern Hemisphere continents have a weak positive
305 effect, leading to slightly warmer conditions relative to a symmetric Earth.

306 Next we try to observe the interhemispheric effect on ΔPDD for a *transition* from SHSP to NHSP
307 orbit. Thus the Interhemispheric effect of Southern Hemisphere continental geography on
308 Northern Hemisphere response to a precession cycle is:

$$309 \quad (\widehat{e_{PDD}})_{precession} = \Delta PDD_{precession}^{control} - \Delta PDD_{precession}^{north} \quad \dots(9)$$

310 The calculated effect is plotted spatially in Figure 6A, and shows a strong negative effect
311 on Northern Hemisphere PDDs. For the Northern Hemisphere, the transition from SHSP
312 to NHSP equates to a transition from cool to warm climate. The negative
313 interhemispheric effect decreases the ΔPDD in the real Earth, thus weakening the effect
314 of precession on the Northern Hemisphere.

315 The effect of Southern Hemisphere continental geography on NH climate response at the
316 two extreme obliquity orbits are estimated as:

$$317 \quad (\widehat{e_{PDD}})_{HIGH} = PDD_{HIGH}^{control} - PDD_{HIGH}^{north} \quad \dots(10)$$

318 and



$$319 \quad (\widehat{e_{PDD}})_{LOW} = PDD_{LOW}^{control} - PDD_{LOW}^{north} \quad \dots(11)$$

320 At HIGH obliquity, there exists a negative effect on Northern Hemisphere continents
321 (Fig. 5C), which mutes the strong insolation intensity during summer months. In the
322 Northern Hemisphere, as a result of continental asymmetry, a decrease in the equator to
323 pole temperature gradient is observed. A lowering of summer temperatures and
324 temperature gradient due to the interhemispheric effect has a negative impact on the
325 deglaciation trigger associated with HIGH obliquity orbits. Thus the interhemispheric
326 effect would hinder the melting of ice during high-obliquity orbits. At LOW obliquity,
327 the negative effect over Northern Hemisphere continents is generally less intense (Fig.
328 5D). However, even the modest lowering of summer temperatures caused by the
329 interhemispheric effect would support the growth of ice sheets during low obliquity
330 orbits.

331 Further, we calculate the interhemispheric effect on ΔPDD for a transition from LOW to
332 HIGH orbit (obliquity cycle). This Interhemispheric effect of Southern Hemisphere
333 continental geography on Northern Hemisphere response to an obliquity cycle is:

$$334 \quad (\widehat{e_{PDD}})_{obliquity} = \Delta PDD_{obliquity}^{control} - \Delta PDD_{obliquity}^{north} \quad \dots(12)$$

335 The calculated effect is spatially plotted in Figure 6C, and shows a small negative effect
336 in the high latitudes, and a positive effect in the low latitudes. The transition from LOW
337 to HIGH corresponds to a transition from cold to warm climate. The negative
338 interhemispheric effect decreases the ΔPDD , thus weakening the climate response of
339 obliquity cycle in the high latitudes. The positive interhemispheric effect increases the



340 ΔPDD , thus strengthening the climate response of obliquity cycle in the Northern
341 Hemisphere low latitudes.

342 5.2 Effect of Northern Hemisphere geography on Southern Hemisphere climate

343 The effect of Northern Hemisphere continental geography on SH climate response at two
344 extreme precessional orbits is estimated as:

$$345 \quad (\widehat{e_{PDD}})_{NHSP} = PDD_{NHSP}^{control} - PDD_{NHSP}^{south} \quad \dots(13)$$

346 and

$$347 \quad (\widehat{e_{PDD}})_{SHSP} = PDD_{SHSP}^{control} - PDD_{SHSP}^{south} \quad \dots(14)$$

348 The spatial variation of $(\widehat{e_{PDD}})_{NHSP}$ is shown in Figure 5E. During NHSP orbit, the
349 Southern Hemisphere experiences ‘glacial’ (cold summer) conditions due to the weaker
350 summer insolation. The positive effect in the Southern Hemisphere leads to weaker
351 cooling relative to a symmetric Earth. Thus, when perihelion coincides with Northern
352 Hemisphere summer, the interhemispheric effect dampens the magnitude of ‘glacial’
353 versus ‘interglacial’ conditions in both hemispheres. When perihelion coincides with
354 Southern Hemisphere summer (SHSP), the southern high latitudes experience intense
355 summer insolation. The positive warming effect (Fig. 5F) amplifies the ‘interglacial’
356 conditions in the Southern Hemisphere, predicted by Milankovitch theory.

357 The interhemispheric effect on ΔPDD for a transition from SHSP to NHSP orbit, or the
358 interhemispheric effect of Northern Hemisphere continental geography on Southern
359 Hemisphere response to a precession cycle is:



$$360 \quad (\widehat{e_{PDD}})_{precession} = \Delta PDD_{precession}^{control} - \Delta PDD_{precession}^{south} \quad \dots(15)$$

361 The calculated effect is plotted spatially in Figure 6B, and shows a positive effect on
362 PDD over Southern Hemisphere high latitudes. For the Southern Hemisphere, the
363 transition from SHSP to NHSP equates to a transition from warmer to cooler climate. The
364 positive interhemispheric effect at high latitudes decreases the $|\Delta PDD|$ in the real Earth,
365 thus weakening the effect of precessional cycle in the Southern Hemisphere high
366 latitudes.

367 The interhemispheric effect of Northern Hemisphere continental geography on Southern
368 Hemisphere climate at the two extreme obliquity configurations is calculated as:

$$369 \quad (\widehat{e_{PDD}})_{HIGH} = PDD_{HIGH}^{control} - PDD_{HIGH}^{south} \quad \dots(16)$$

370 and

$$371 \quad (\widehat{e_{PDD}})_{LOW} = PDD_{LOW}^{control} - PDD_{LOW}^{south} \quad \dots(17)$$

372 The spatial variations of $(\widehat{e_{PDD}})_{HIGH}$ and $(\widehat{e_{PDD}})_{LOW}$ are shown in Figure 5G and 5H,
373 respectively. In the Southern Hemisphere, the positive interhemispheric effect on PDD
374 over Antarctica and the Southern Ocean leads to overall higher temperatures in the high
375 southern latitudes as compared to a symmetric Earth. During high obliquity orbits, this
376 positive effect contributes to deglaciation and during low obliquity orbits; the positive
377 effect (warming) hinders the growth of ice sheets.

378 Lastly, we calculate the interhemispheric effect on ΔPDD for a transition from LOW to
379 HIGH orbit (obliquity cycle):



$$380 \quad (\widehat{\bar{e}_{PDD}})_{obliquity} = \Delta PDD_{obliquity}^{control} - \Delta PDD_{obliquity}^{south} \quad \dots(18)$$

381 The calculated effect is plotted in Figure 6D, and shows largely a negative effect in the
382 Southern Hemisphere, with a positive effect in the high latitudes. The transition from
383 LOW to HIGH corresponds to a transition from cold to warm climate. The positive
384 interhemispheric effect increases the ΔPDD , thus amplifying the effect of obliquity over
385 Antarctica.

386 6. Conclusions

387 The unbalanced fraction of land in the Northern versus Southern Hemisphere has
388 remained almost unchanged for tens of millions of years. However, the significance of
389 this continental asymmetry on Earth's climate response to forcing has not been
390 previously quantified with a physically based climate models. We find that continental
391 geography has an important control on the climate system's response to insolation
392 forcing, and this may help explain the non-linear response of the Earth's climate to
393 insolation forcing.

394 According to classical Milankovitch theory, the growth of polar ice sheets at the onset of
395 glaciation requires cooler summers in the high latitudes, in order for snow to persist
396 throughout the year. During warm summers at the high latitudes, the winter snowpack
397 melts, inhibiting glaciation or leading to deglaciation if ice sheets already exist. Thus, the
398 intensity of summer insolation at high latitudes, especially the Northern polar latitudes,
399 has been considered the key driver of the glacial-interglacial cycles and other long-term
400 climatic variations. At precessional periods, at which the high latitude summer intensity



401 primarily varies, the land asymmetry effect plays an important role by amplifying (or
402 weakening) the effect of summer insolation intensity.

403 In all the orbital configurations simulated here, we find that the geography of the
404 Southern Hemisphere weakens the temperature response of the high Northern
405 Hemisphere latitudes to orbital forcing. Consequently, this leads to a larger latitudinal
406 gradient in summer temperatures in the Northern Hemisphere compared to that of a
407 symmetric Earth. In particular, the amplification (or weakening) of the response to
408 insolation changes at precessional and obliquity periods might explain some of the
409 important features of late Pliocene-early Pleistocene climate variability, when obliquity-
410 paced cyclicality dominated precession in global benthic $\delta^{18}\text{O}$ records. In Figure 6, we have
411 demonstrated that the interhemispheric effect causes a suppression of the effects of
412 precessional cycle on the Earth's surface. In other words, the real Earth has a smaller
413 response to a precession cycle as compared to the hypothetical symmetric Earth. We have
414 also showed that the interhemispheric effect causes an amplification of the effects of
415 obliquity cycle on the Earth's surface. In other words, the real Earth has a larger response
416 to the obliquity cycle in the ocean dominated Southern Hemisphere, as compared to the
417 hypothetical symmetric Earth. Consequently, the interhemispheric effect of continental
418 geography contributes to the muting of precessional signal and amplification of obliquity
419 signal recorded in paleoclimate proxies such as benthic $\delta^{18}\text{O}$ isotope records.

420 There are various ways in which the Earth's continental asymmetry affects climate. Here,
421 we have shown how these interhemispheric effects influence the Earth's climate response
422 to orbital forcing via the radiative and atmospheric dynamical processes represented in a



423 slab-ocean GCM. While computationally challenging, future work should include
424 complimentary simulations with AOGCMs, to explore the potential modifying role of
425 ocean dynamics on the amplifying and weakening interhemispheric responses to orbital
426 forcing demonstrated here.



427 **Table 1. Experimental Setup of Model Boundary Conditions and Forcings**

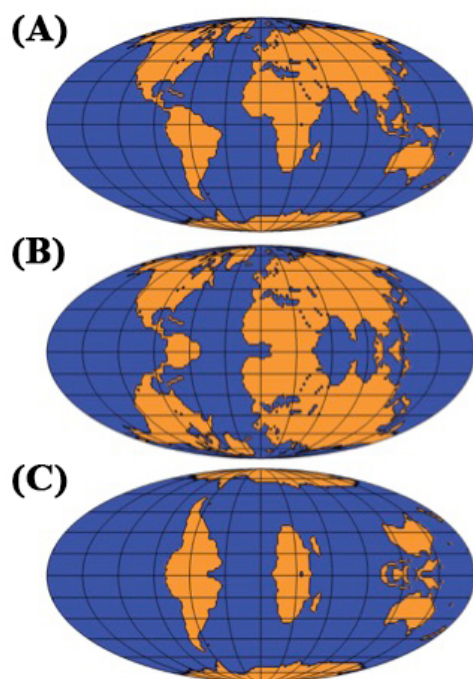
Run ID	LSX Configuration	Eccentricity	Obliquity	Precession ^a	GHGs
CONTROL _{NHSP}	Modern	0.034	23.2735	270° (NHSP)	Preindustrial
CONTROL _{SHSP}	Modern	0.034	23.2735	90° (SHSP)	Preindustrial
CONTROL _{HIGH}	Modern	0.034	24.5044	180°	Preindustrial
			(HIGH)		
CONTROL _{LOW}	Modern	0.034	22.0425	180°	Preindustrial
			(LOW)		
NORTH-SYMM _{NHSP}	North-symmetric	0.034	23.2735	270° (NHSP)	Preindustrial
NORTH-SYMM _{SHSP}	North-symmetric	0.034	23.2735	90° (SHSP)	Preindustrial
NORTH-SYMM _{HIGH}	North-symmetric	0.034	24.5044	180°	Preindustrial
			(HIGH)		
NORTH-SYMM _{LOW}	North-symmetric	0.034	22.0425	180°	Preindustrial
			(LOW)		
SOUTH-SYMM _{NHSP}	South-symmetric	0.034	23.2735	270° (NHSP)	Preindustrial
SOUTH-SYMM _{SHSP}	South-symmetric	0.034	23.2735	90° (SHSP)	Preindustrial
SOUTH-SYMM _{HIGH}	South-symmetric	0.034	24.5044	180°	Preindustrial
			(HIGH)		
SOUTH-SYMM _{LOW}	South-symmetric	0.034	22.0425	180°	Preindustrial
			(LOW)		

428 **NHSP:** Northern Hemisphere Summer Solstice at Perihelion

429 **SHSP:** Southern Hemisphere Summer Solstice at Perihelion

430 ^a Orbital precession in the GCM is defined here as the prograde angle from perihelion to

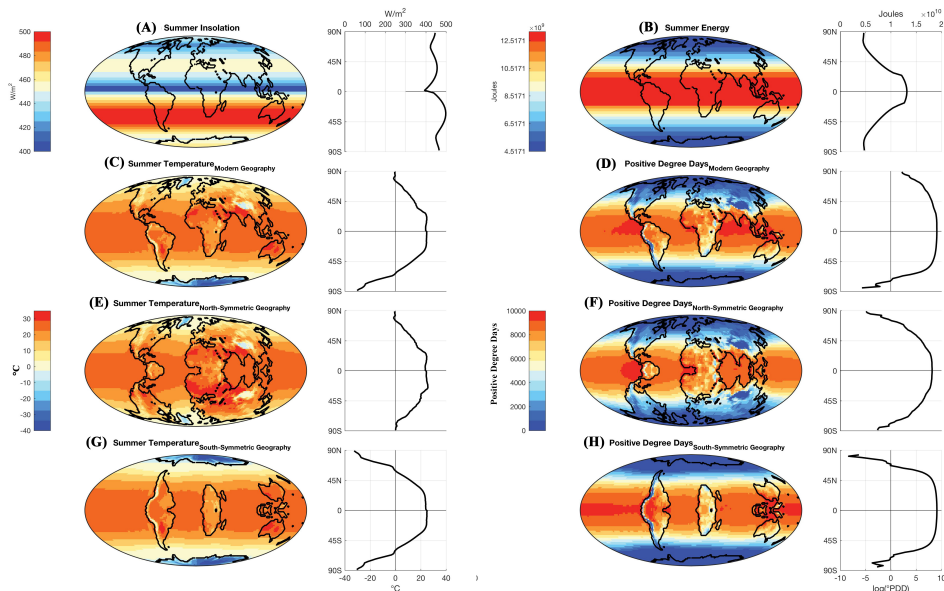
431 the Northern Hemispheric vernal equinox.



432

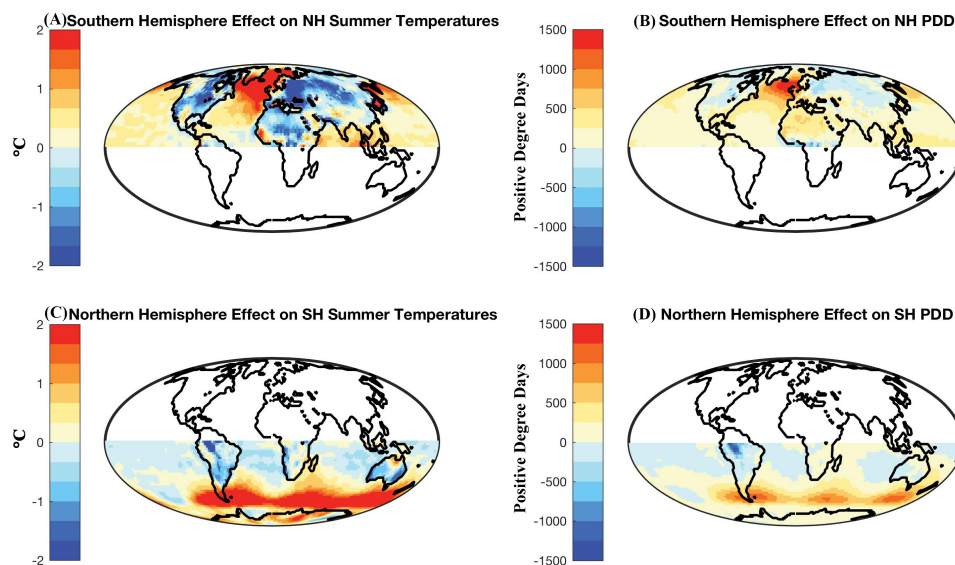
433 **Figure 1.** (A) Modern continental geography (B) NORTH-SYMM geography and (C)

434 SOUTH-SYMM geography



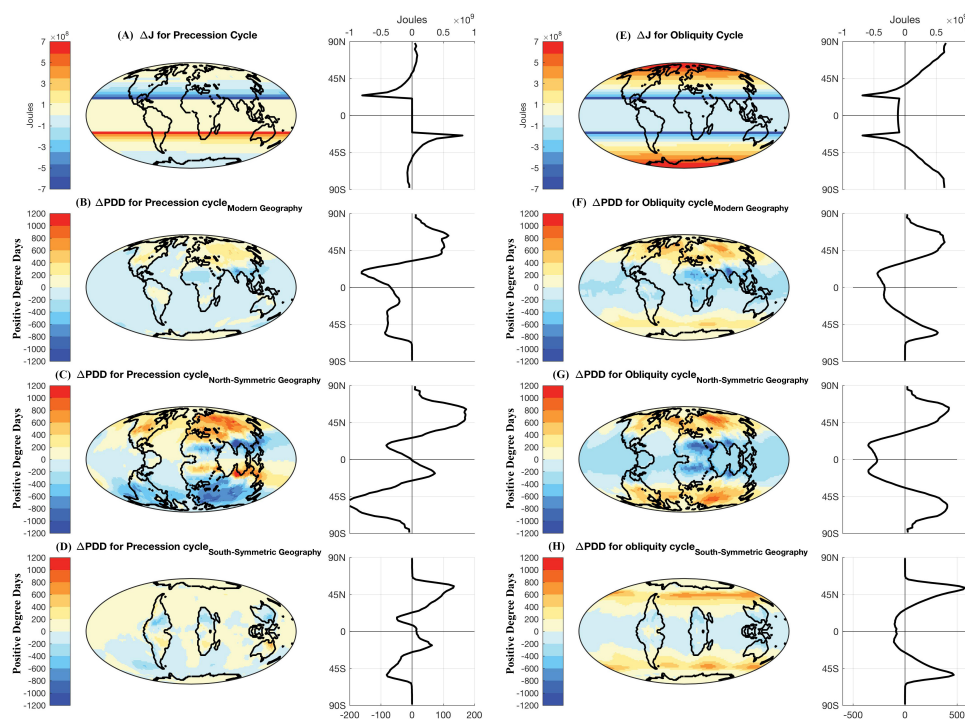
435

436 **Figure 2.** (A-D) Demonstration of Earth’s asymmetric climate response to symmetric
 437 climate forcing. Simulations are forced by modern day orbit: (A) Summer insolation; (B)
 438 summer energy; (C) Summer Temperature; and (D) PDD. (E-H) Demonstration of
 439 Earth’s symmetric climate response to climate forcing when idealized symmetric Earth
 440 geographies are used. Simulations are forced by modern day orbit: (E) and (F) Summer
 441 Temperature and PDD for NORTH-SYMM simulation, (G) and (H) Summer
 442 Temperature and PDD for SOUTH-SYMM simulation. The zonal averages are plotted on
 443 the right of each Figure. Zonal averages of PDD are plotted on a log scale.



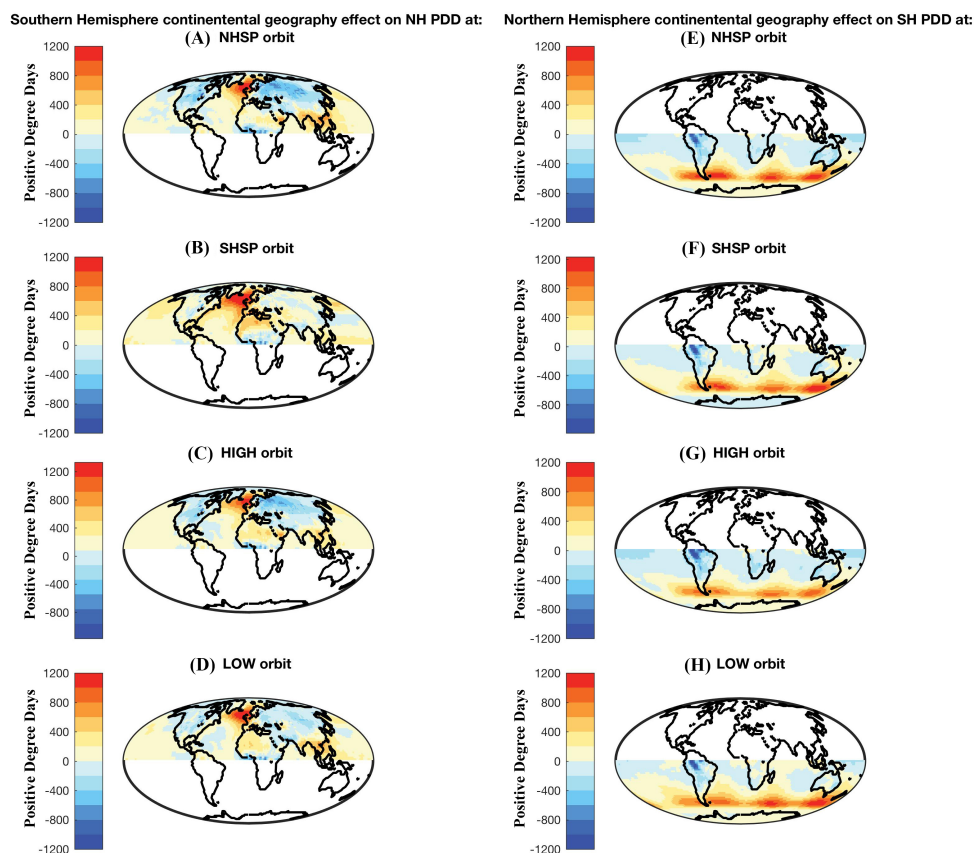
444

445 **Figure 3.** Interhemispheric effect of Southern Hemisphere continental geography on (A)
446 Northern Hemisphere Summer Temperature (ST) and (B) Positive Degree Days (PDD).
447 Interhemispheric effect of Northern Hemisphere continental geography on (C) Southern
448 Hemisphere Summer Temperature (ST) and (D) Positive Degree Days (PDD). Zonal
449 averages are plotted on the right of each figure.



450

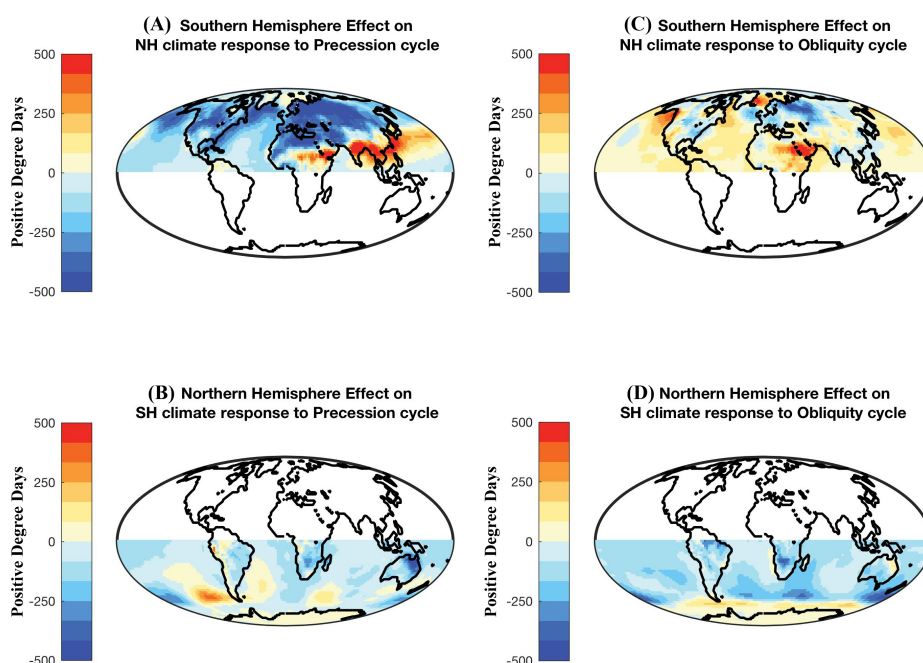
451 **Figure 4.** (A) Summer Energy change for a transition from SHSP to NHSP orbit and the
 452 corresponding change in Positive Degree Days in CONTROL (B); NORTH-SYMM (C)
 453 and SOUTH-SYMM (D) simulations. (E) Summer Energy change for a transition from
 454 LOW to HIGH orbit and the corresponding change in PDD in CONTROL (F); NORTH-
 455 SYMM (G) and SOUTH-SYMM (H) simulations.



456

457 **Figure 5.** Interhemispheric effect of Southern Hemisphere continental geography on
 458 Northern Hemisphere climate: (A) at NHSP $[(\widehat{e}_{PDD})_{NHSP}]$; (B) at SHSP $[(\widehat{e}_{PDD})_{SHSP}]$;
 459 (C) at HIGH $[(\widehat{e}_{PDD})_{HIGH}]$; (D) at LOW $[(\widehat{e}_{PDD})_{LOW}]$.

460 Interhemispheric effect of Northern Hemisphere continental geography on Southern
 461 Hemisphere climate: (E) at NHSP $[(\widehat{e}_{PDD})_{NHSP}]$; (F) at SHSP $[(\widehat{e}_{PDD})_{SHSP}]$; (G) at HIGH
 462 $[(\widehat{e}_{PDD})_{HIGH}]$; (H) at LOW $[(\widehat{e}_{PDD})_{LOW}]$.



463

464 **Figure 6.** Interhemispheric effect of: (A) Southern Hemisphere continental geography on
 465 Northern Hemisphere $\Delta PDD_{precession}$ (response to precession forcing) $[(\widehat{e_{PDD}})_{precession}]$,
 466 (B) Northern Hemisphere continental geography on Southern Hemisphere $\Delta PDD_{precession}$
 467 (response to precession forcing) $[(\widehat{e_{PDD}})_{precession}]$, (C) Southern Hemisphere continental
 468 geography effect on Northern Hemisphere $\Delta PDD_{obliquity}$ (response to Obliquity)
 469 $[(\widehat{e_{PDD}})_{obliquity}]$, (D) Northern Hemisphere continental geography effect on Southern
 470 Hemisphere $\Delta PDD_{obliquity}$ (response to Obliquity) $[(\widehat{e_{PDD}})_{obliquity}]$.



- 471 Alder, J. R., Hostetler, S. W., Pollard, D. and Schmittner, A.: Evaluation of a present-day climate
472 simulation with a new coupled atmosphere-ocean model GENMOM, *Geosci. Model Dev.*, 4(1),
473 69–83, doi:10.5194/gmd-4-69-2011, 2011.
- 474 Barron, E. J., Thompson, S. L. and Hay, W. W.: Continental distribution as a forcing factor for
475 global-scale temperature, *Nature*, 310(5978), 574–575, doi:10.1038/310574a0, 1984.
- 476 Berger, A. and Loutre, M. F.: Insolation values for the climate of the last 10 million years, *Quat.*
477 *Sci. Rev.*, 10(4), 297–317, doi:10.1016/0277-3791(91)90033-Q, 1991.
- 478 Croll, J.: No Title, *Philos. Mag. J. Sci.*, 39(259), 81–106, 1870.
- 479 Crowley, T. J. and North, G. R.: *Paleoclimatology*, Oxford University Press. [online] Available
480 from: [http://books.google.com/books/about/Paleoclimatology.html?id=VDE-](http://books.google.com/books/about/Paleoclimatology.html?id=VDE-mKySpM0C&pgis=1)
481 [mKySpM0C&pgis=1](http://books.google.com/books/about/Paleoclimatology.html?id=VDE-mKySpM0C&pgis=1) (Accessed 13 November 2014), 1996.
- 482 DeConto, R.: Plate Tectonics and Climate Change, in *Encyclopedia of Paleoclimatology and*
483 *Ancient Environments SE - 188*, edited by V. Gornitz, pp. 784–798, Springer Netherlands., 2009.
- 484 Deconto, R. M., Pollard, D., Wilson, P. A., Pälike, H., Lear, C. H. and Pagani, M.: Thresholds for
485 Cenozoic bipolar glaciation., *Nature*, 455(7213), 652–6, doi:10.1038/nature07337, 2008.
- 486 Fawcett, P. J. and Barron, E. J.: The Role of Geography and Atmospheric CO₂ in Long Term
487 Climate Change: Results from Model Simulations for the Late Permian to the Present, in *Tectonic*
488 *Boundary Conditions for Climate Reconstructions*, pp. 227–247, Oxford University Press., 1998.
- 489 Flato, G. M. and Boer, G. J.: Warming asymmetry in climate change simulations, *Geophys. Res.*
490 *Lett.*, 28(1), 195–198, doi:10.1029/2000GL012121, 2001.
- 491 Hay, W. W.: Tectonics and climate, *Geol. Rundschau*, 85(3), 409–437, doi:10.1007/BF02369000,
492 1996.
- 493 Hay, W. W., Barron, E. J. and Thompson, S. L.: Results of global atmospheric circulation
494 experiments on an Earth with a meridional pole-to- pole continent, *J. Geol. Soc. London.*, 147(2),



- 495 385–392, doi:10.1144/gsjgs.147.2.0385, 1990.
- 496 Huybers, P.: Early Pleistocene glacial cycles and the integrated summer insolation forcing.,
497 Science, 313(5786), 508–11, doi:10.1126/science.1125249, 2006.
- 498 Kang, S. M., Held, I. M., Frierson, D. M. W. and Zhao, M.: The Response of the ITCZ to
499 Extratropical Thermal Forcing: Idealized Slab-Ocean Experiments with a GCM, J. Clim., 21(14),
500 3521–3532, doi:10.1175/2007JCLI2146.1, 2008.
- 501 Kang, S. M., Seager, R., Frierson, D. M. W. and Liu, X.: Croll revisited: Why is the northern
502 hemisphere warmer than the southern hemisphere?, Clim. Dyn., 1457–1472, doi:10.1007/s00382-
503 014-2147-z, 2014.
- 504 Kiehl, J. T., Hack, J. J., Bonan, G. B., Boville, B. a., Williamson, D. L. and Rasch, P. J.: The
505 National Center for Atmospheric Research Community Climate Model: CCM3*, J. Clim., 11(6),
506 1131–1149, doi:10.1175/1520-0442(1998)011<1131:TNCFAR>2.0.CO;2, 1998.
- 507 Koenig, S. J., DeConto, R. M. and Pollard, D.: Pliocene Model Intercomparison Project
508 Experiment 1: implementation strategy and mid-Pliocene global climatology using GENESIS
509 v3.0 GCM, Geosci. Model Dev., 5(1), 73–85, doi:10.5194/gmd-5-73-2012, 2012.
- 510 Loutre, M.-F., Paillard, D., Vimeux, F. and Cortijo, E.: Does mean annual insolation have the
511 potential to change the climate?, Earth Planet. Sci. Lett., 221(1–4), 1–14, doi:10.1016/S0012-
512 821X(04)00108-6, 2004.
- 513 Loutre, M. F.: Clues from MIS 11 to predict the future climate – a modelling point of view, Earth
514 Planet. Sci. Lett., 212(1–2), 213–224, doi:10.1016/S0012-821X(03)00235-8, 2003.
- 515 Philander, S. G. H., Gu, D., Lambert, G., Li, T., Halpern, D., Lau, N.-C. and Pacanowski, R. C.:
516 Why the ITCZ Is Mostly North of the Equator, J. Clim., 9(12), 2958–2972, doi:10.1175/1520-
517 0442(1996)009<2958:WTIIMN>2.0.CO;2, 1996.
- 518 Raymo, M. E., Lisiecki, L. E. and Nisancioglu, K. H.: Plio-Pleistocene Ice Volume, Antarctic



- 519 Climate, and the Global d18O Record, , 313(July), 492–495, 2006.
- 520 Short, D. A., Mengel, J. G., Crowley, T. J., Hyde, W. T. and North, G. R.: Filtering of
521 Milankovitch Cycles by Earth’s Geography, *Quat. Res.*, 35(2), 157–173, doi:10.1016/0033-
522 5894(91)90064-C, 1991.
- 523 Stone, P. H.: Constraints on dynamical transports of energy on a spherical planet, *Dyn. Atmos.*
524 *Ocean.*, 2(2), 123–139, doi:10.1016/0377-0265(78)90006-4, 1978.
- 525 Stouffer, R. J., Manabe, S. and Bryan, K.: Interhemispheric asymmetry in climate response to a
526 gradual increase of atmospheric CO₂, *Nature*, 342(6250), 660–662, doi:10.1038/342660a0, 1989.
- 527 Thompson, S. L. and Pollard, D.: Greenland and Antarctic Mass Balances for Present and
528 Doubled Atmospheric CO₂ from the GENESIS Version-2 Global Climate Model, *J. Clim.*,
529 10(5), 871–900, doi:10.1175/1520-0442(1997)010<0871:GAAMBF>2.0.CO;2, 1997.
- 530 Trenberth, K. E., Fasullo, J. T. and Kiehl, J.: Earth’s Global Energy Budget, *Bull. Am. Meteorol.*
531 *Soc.*, 90(3), 311–323, doi:10.1175/2008BAMS2634.1, 2009.
- 532